Sensitivity of a Model Shelfbreak Front to the Parameterization of Vertical Mixing*

DAVID C. CHAPMAN

Woods Hole Oceanographic Institution, Woods Hole, Massachusetts

2 January 2002 and 4 June 2002

ABSTRACT

Recent observations have suggested that the trapped-front model of Chapman and Lentz is consistent with some aspects of the shelfbreak front in the Middle Atlantic Bight. The sensitivity of the model to the parameterization of vertical mixing is examined to determine which model features are robust and potentially observable and which are variable and less reliable. The basic frontal trapping mechanism, frontal location, surface intensified frontal jet with weak flow at the bottom, and detachment of the bottom boundary layer at the shoreward edge of the foot of the front are all insensitive to the parameterization of vertical mixing. On the other hand, the frontal shape and width and the cross-frontal circulation and momentum balances within the front change dramatically with the parameterization of vertical mixing. Constant mixing coefficients produce strong vertical mixing within the front, which results in steady shoreward flow in the bottom boundary layer there. Mixing coefficients that depend on the local stratification and shear produce weak vertical mixing within the front, which allows oscillating currents that may be frontal-trapped waves.

1. Introduction

The exchange of heat, salt, mass, nutrients, carbon, and pollutants between the shelf and the deep ocean is presently a topic of much interest, but it remains poorly understood. Shelf-edge flows are complicated because numerous processes contribute and often act simultaneously. In addition, some shelf edges are dominated by a persistent shelfbreak front whose dynamics are still largely a mystery. For example, the Middle Atlantic Bight (MAB) shelf edge and shelfbreak front have been studied extensively for more than two decades, yet there is much uncertainty about shelf-edge exchange there, including its magnitude, location, and timing (e.g. Loder et al. 1998).

Numerous attempts have been made to model a shelfbreak front, and these have been briefly reviewed by Chapman (2000). Despite these efforts, it is fair to say that no model fully reproduces the observed behavior of a shelfbreak front. At best, models suggest some gross features of frontal behavior. Some attention recently has been given to the highly idealized trapped-front model of Chapman and Lentz (1994), which was designed to study the development of a surface-to-bottom density front driven by a buoyant coastal source. In this model, the action of downslope buoyancy advection in the bottom boundary layer moves the entire front offshore until the water is deep enough that the vertical (thermal wind) shear in the alongfront velocity reverses the velocity at the bottom within the front (Fig. 1). The Ekman transport in the bottom boundary layer also reverses there, creating a convergence in the bottom boundary layer at the shoreward side of the foot of the front,[1] where the boundary layer detaches (or separates) from the bottom. The front is trapped along this isobath, and Yankovsky and Chapman (1997) showed that the trapping depth h_b is given by

$$h_b = (2fT/g')^{1/2}, \tag{1}$$

where f is the Coriolis parameter, T is the transport in the front, and $g' = g\Delta\rho/\rho_0$ is reduced gravity, with g being gravitational acceleration, $\Delta\rho$ the density difference across the front, and ρ_0 the mean density. The trapped-front model was not originally intended to model a shelfbreak front, but Chapman (2000) showed that the trapping mechanism operates at depths of typical shelfbreaks (100–150 m) and that (1) remains a good predictor of the trapping depth.

Recent observations near and within the MAB shelfbreak front support some features of the trapped-front

* Woods Hole Oceanographic Institution Contribution Number 10591.

Corresponding author address: David C. Chapman, Woods Hole Oceanographic Institution, MS #21, Woods Hole, MA 02543.
E-mail: dchapman@whoi.edu

[1] The foot of the front is defined here as the entire region where the front intersects the bottom topography.

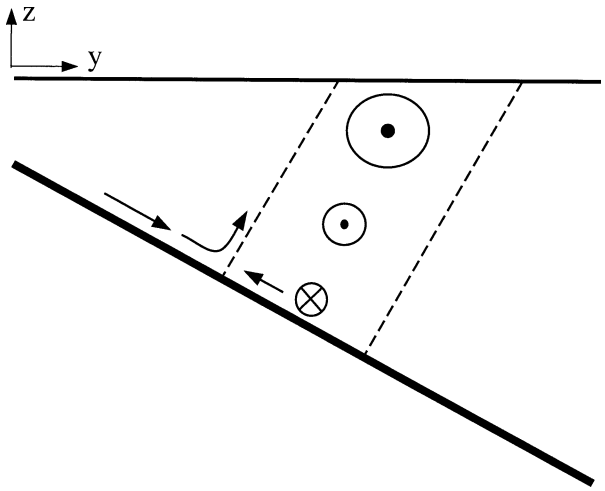

FIG. 1. Schematic cross-shelf section of the trapped-front model, showing a surface-to-bottom front (between the dashed lines) with a surface intensified alongfront jet (⊙). The along-isobath flow reverses at the bottom (⊗), producing shoreward flow within the foot of the front. Convergence in the bottom boundary layer causes detachment, with flow upward along isopycnals.

model. For example, Houghton (1997) released dye near the bottom within the foot of the MAB shelfbreak front and followed the dye patch as it moved shoreward, with the patch largely remaining in the bottom boundary layer. Although the foot of the front itself moved shoreward, Houghton (1997) found that the dye moved shoreward faster than the front. He argued that this observation is consistent with the shoreward flow in the model bottom boundary layer beneath the trapped front (Fig. 1). Houghton and Visbeck (1998) later released dye in the bottom boundary layer on the shoreward side of the front and followed it as it moved upward, out of the bottom boundary layer and along isotherms, until it reached the central part of the front. This behavior is consistent with the bottom boundary layer detachment in the trapped-front model. Additional support for the detachment comes from elevated levels of chlorophyll and suspended material, emanating from the bottom boundary layer and extending upward along the shoreward side of the MAB shelfbreak front (Barth et al. 1998). Further, Pickart (2000) devised an analysis technique, using temperature variations along isopycnals from hydrographic measurements, that reveals evidence of a detached bottom boundary layer at the MAB shelfbreak front. His results are consistent with both shipboard velocity measurements and the trapped-front model.

Considering both the idealized nature of the trapped-front model (e.g., simple inflow and topography, and lack of other forcing mechanisms) and the apparent relevance of the model to observed shelfbreak fronts, it makes sense to ask how seriously to believe the details of the model dynamics. That is, which model features might one expect to observe in a shelfbreak front, and which features are the result of model assumptions? One approach to addressing these questions is to explore the sensitivity of the model results to particular assumptions and idealizations in order to determine which features are robust and which are not. For example, the effects of wind forcing, tidal forcing, offshore forcing, topographic variations, or inflow variability could be investigated. However, in some sense, these are each external to the dynamics of the trapped front itself. Instead, the focus here is on the sensitivity of the trapped-front model to the parameterization of vertical mixing, which represents an intrinsic and fundamental fluid behavior and is probably the most poorly defined model property.

Many schemes have been proposed for the parameterization of vertical mixing, but none is generally accepted as the most realistic. Yet the parameterization of vertical mixing is expected to have important consequences on the dynamics of the trapped-front model. For instance, the stress condition at the bottom is

$$A_V u_z = ru \quad \text{at } z = -h, \tag{2}$$

where A_V is the vertical viscosity, u is the along-isobath velocity, z is the vertical coordinate, r is a linear bottom friction coefficient, h is the depth, and subscript z denotes partial differentiation. The front is trapped at the location where $u = 0$ at the shoreward side of the foot of the front. This implies that the along-isobath component of bottom stress also vanishes; that is, either A_V or u_z must vanish from (2). The along-isobath velocity u tends to be in thermal wind balance through most of the water column, so u_z is basically set by the cross-isobath density gradient and is typically nonzero within the front. Therefore, bottom stress can vanish within the front only if A_V vanishes. However, if the mixing parameterization restricts A_V so that it cannot vanish at the bottom, then vanishing bottom stress is incompatible with thermal wind balance, and other dynamics must become important.

Chapman and Lentz (1994) chose the extreme idealization of constant A_V, which clearly cannot vanish at the bottom. As a consequence, the reversal of the along-isobath flow beneath the front produces a classical Ekman bottom boundary layer with onshore flow under most of the front, which sets up a convergence at the shoreward side of the foot of the front with oppositely directed cross-front velocities (Fig. 1). Chapman (2000), on the other hand, used the Mellor–Yamada level-2 (MY2; Mellor and Yamada 1982) turbulence closure scheme in which vertical mixing coefficients are estimated based on the local Richardson number. This scheme is one of many that attempts to reproduce the tendency for ocean mixing to increase in the presence of large current shears and/or weak stratification. With MY2, A_V can vanish near the bottom, so both vanishing bottom stress and thermal wind balance can occur simultaneously. The cross-front velocity need not reverse beneath the front to cause the detachment of the bottom boundary layer [see Fig. 4 of Chapman (2000)]. That

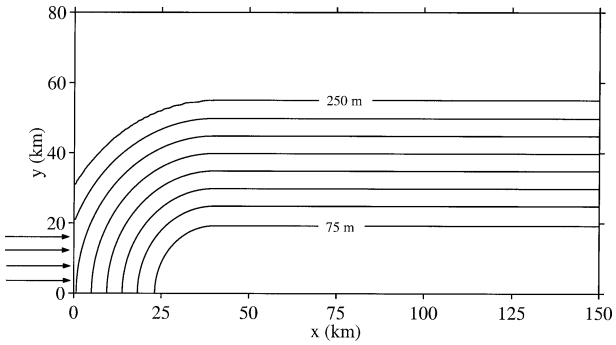

FIG. 2. Plan view of the numerical model domain with isobaths. Arrows on the left between $y = 0$ and 20 km indicate the location of the buoyant inflow.

is, a sufficiently small along-isobath bottom velocity within the foot of the front can reduce the cross-isobath Ekman transport enough to produce a strong convergence and, hence, detachment. This suggests the possibility of very different dynamics within the front in comparison with those of the Chapman and Lentz (1994) model.

This paper compares and contrasts the trapped-front model produced using (i) constant mixing coefficients and (ii) the MY2 turbulence closure scheme. Additional calculations have been made for this comparison using other parameterizations, but the model sensitivity is clearly demonstrated from these two choices. The aim is to determine which model features are robust and perhaps observable and to provide a word of caution regarding interpretation of observations in terms of model flows.

2. Numerical model

For both parameterizations of vertical mixing, the trapped front is generated using the Semi-Spectral Primitive Equation Model, version 5.1 (SPEM5.1) in almost exactly the same configuration as Chapman (2000), so only a brief description is given here. SPEM5.1 solves the standard hydrostatic and Boussinesq momentum, density, and continuity equations. The model domain (Fig. 2) is a uniformly rotating straight channel with solid walls at the coast ($y = 0$) and offshore ($y = 80$ km) and open boundaries at $x = 0$ and $x = 150$ km. The bottom is nearly flat at the upstream end ($x = 0$), rises rapidly in the x direction, and becomes invariant in x for the remainder of the channel; that is, the isobaths become parallel to the coast. The horizontal grid resolution is twice that of Chapman (2000): uniform grid spacing of $\Delta x = 0.78$ km and $\Delta y = 0.83$ km.

Standard dynamical assumptions are made: rigid lid, no flow or density flux through solid boundaries, linearized bottom stress with a bottom friction coefficient of 5×10^{-4} m s^{-1}, and convective adjustment to mix statically unstable density distributions. Laplacian subgrid-scale horizontal mixing is used for numerical stability, with small coefficients of 25 m^2 s^{-1} for momentum and 5 m^2 s^{-1} for density; its effects are neglible in the momentum and density balances.

Each calculation begins from rest. A constant buoyant inflow with transport T and density anomaly $\Delta\rho$ is prescribed at $t = 0$ at the upstream boundary ($x = 0$). The remainder of the fluid has constant density. The buoyant inflow is chosen to produce a trapped front along the 150-m isobath according to (1); $f = 10^{-4}$ s^{-1}, $T = 0.33 \times 10^6$ m^3 s^{-1}, $\Delta\rho = 0.3$ kg m^{-3}, and $\rho_0 = 1000$ kg m^{-3}. The bottom slope is 0.005 in the trapping region. A uniform inflow of 0.025 m s^{-1} is imposed at the upstream boundary to stabilize the front at the surface. A radiation condition is applied at the downstream boundary ($x = 150$ km). The model is run for 100 days, by which time a steady state has been reached everywhere in the channel. Other details may be found in Chapman (2000).

To reproduce the Chapman and Lentz (1994) trapped-front model, vertical viscosity and diffusivity are both set at 10^{-3} m^2 s^{-1}. This value is much larger than estimates from observations above the bottom boundary layer (e.g., Houghton and Visbeck 1998) but is smaller than estimates from within oceanic bottom boundary layers (e.g., Sanford and Lien 1999; Stahr and Sanford 1999). When using the MY2 scheme, as described by Chapman (2000), the vertical viscosity and diffusivity are restricted between a minimum of 10^{-5} m^2 s^{-1} and a maximum of 10^{-3} m^2 s^{-1}. The maximum is imposed to avoid extremely large values. Calculations with other choices for the minimum and maximum values have been made for this study, but the changes they produce can be easily understood in terms of the two cases presented here.

3. Results

The trapped front develops as described by Chapman (2000). All results presented here are obtained well downstream from the buoyant source and after a sufficiently long time such that the front has essentially equilibrated in its fully trapped state. Instantaneous fields are shown, but the time-mean structures are nearly identical.

a. Circulation

The velocity structure of the trapped front is shown in Fig. 3 for the cases of constant coefficient (left panels) and MY2 (right panels); u is along the isobaths (positive out of the page), v is across the isobaths (positive to the right), and w is vertical (positive upward). The thick dashed curves indicate the edges of the front; isopycnals are roughly uniformly distributed within the front.

In some ways the basic structure of the two trapped fronts is the same. In both cases, the shoreward foot of the front is trapped near the 150-m isobath, as predicted by (1). The along-isobath current u is concentrated in

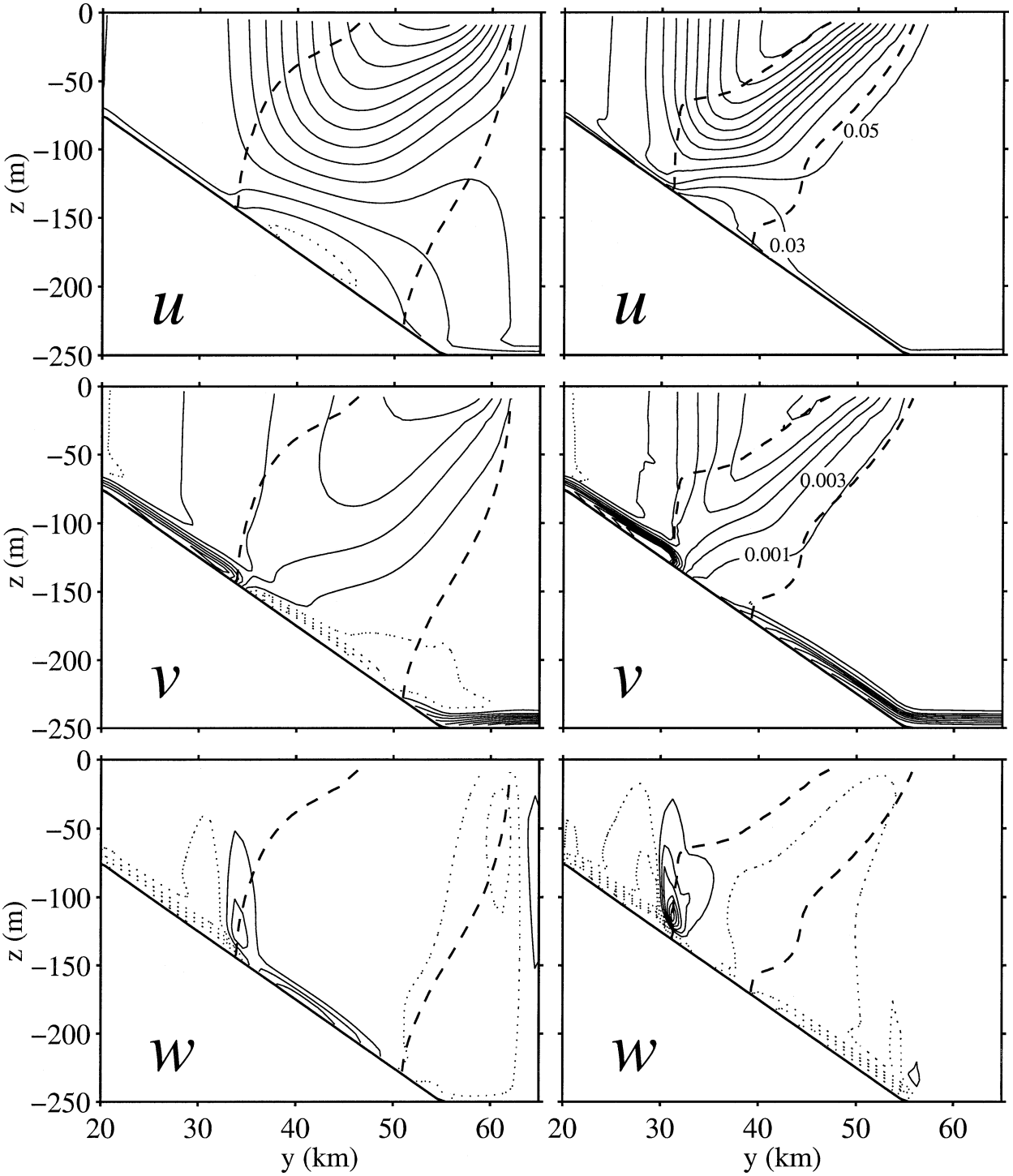

FIG. 3. Vertical slices through the trapped front at $x = 135$ km using (left) constant coefficients and (right) MY2 and showing velocities (m s^{-1}): u is along isobaths (positive out of the page), v is across isobaths (positive to the right), and w is vertical (positive upward). Thick dashed curves indicate the edges of the front. Dotted contours are negative velocities. Contour values are -0.01 to 0.23 by 0.02 for u, -0.007 to 0.017 by 0.002 for v, and -0.8×10^{-4} to 10^{-4} by 1.5×10^{-5} for w.

a surface intensified jet over the front that is vertically sheared with weak flow near the bottom. The surface current structure and relative vorticity (u_y/f; not shown) are nearly the same in both cases. The cross-isobath velocity v tends to be weak (<0.01 m s^{-1}) except in the bottom boundary layer, where it is directed offshore on the shoreward side of the front. (The offshore velocities near the surface indicate that the jet and the surface expression of the front are not quite aligned with the isobaths.) The vertical velocity w shows strong downslope flow in the bottom boundary layer on the shoreward side of the front, which joins a narrow region of strong upward flow at the shoreward edge of the front. This flow corresponds to the detachment of the bottom boundary layer described above. These similarities indicate that the basic frontal trapping mechanism described in the introduction is operating in both cases.

There are also differences between the frontal flows. With MY2, the front is narrower, with more spatial variability. This configuration produces stronger horizontal density gradients and more vertical shear, resulting in a concentration of the frontal transport toward the surface. The upward vertical velocity of the detached bottom boundary layer is considerably stronger with MY2, as is the offshore flow in the bottom boundary layer on the shoreward side of the front.

The velocities within the front are also very different between the two cases. With constant coefficients, the along-isobath velocity near the bottom reverses under the entire front, producing upslope flow in the bottom boundary layer as in Chapman and Lentz (1994) and Fig. 1. With MY2, the along-isobath velocity is small near the bottom, barely reversing in a very small region that is not captured by the chosen contours. As a consequence, the cross-isobath and vertical velocities are weak and downslope nearly everywhere.

b. Density and momentum balances

The density and momentum balances reveal much about the dynamics in the two cases. Figure 4 shows these balances and the vertical viscosity and density, along a line almost parallel to and just above the bottom in Fig. 3 (i.e. the line is 3 m above the bottom at $y = 20$ km and 6 m above the bottom at $y = 60$ km, well within the bottom boundary layer and passing through the foot of the front). The left (right) panels are for constant coefficients (MY2). All of the terms in the momentum and density balances are plotted; the thick curves denote the dominant terms, and the thin curves show terms that are essentially neglible.

The balances are particularly simple with constant coefficients. The density plot (Fig. 4a) shows that the front is located between $y = 35$ and 50 km (shaded region). The along-isobath momentum balance (Fig. 4c) is between the Coriolis force and vertical mixing, $-fv = A_V u_{zz}$; a classical Ekman boundary layer. Notice that when v reverses within the front, the balance is maintained. The cross-isobath momentum balance (Fig. 4d) is everywhere geostrophic regardless of the sign of u; $fu = -p_y/\rho_0$, where p is pressure. The density balance (Fig. 4e) through most of the front is between onshore advection of density, which tends to flatten the front, and vertical mixing, which tends to steepen the front; $v\rho_y = K_V\rho_{zz}$ where ρ is the density anomaly and K_V is the vertical diffusivity. These are the same balances found by Chapman and Lentz (1994), who pointed out that the reversal in v within the front is necessary to maintain a steady state because $K_V\rho_{zz} < 0$.

The situation is very different with MY2. The front is considerably narrower (Fig. 4f), and the vertical viscosity decreases abruptly from the maximum outside the front to the minimum within the front (Fig. 4g). Of interest, the density plot suggests a narrower front than does the minimum in A_V. The density field has adjusted in such a way that u is small (≤ 0.01 m s^{-1}) at the bottom through the entire front (Fig. 3). The abrupt change in A_V appears to be a property of Mellor–Yamada schemes in ocean models; that is, the mixing coefficients revert to their background values when stratification is present (i.e., within the front). Garvine (1999) consistently found the same behavior. As a result, vertical mixing nearly vanishes within the front and does not play a dynamical role there. Shoreward and seaward of the front ($y < 31$ km and $y > 39$ km), the momentum balances are identical to those with constant coefficients. Within the front, all of the terms are much smaller, and the along-isobath momentum balance (Fig. 4h) involves the local acceleration, the Coriolis force, and the pressure gradient: $u_t - fv = -p_x/\rho_0$. The cross-isobath momentum balance (Fig. 4i) is again geostrophic, $fu = -p_y/\rho_0$. The density balance (Fig. 4j) is the simple conservation of density following a fluid parcel, $\rho_t + u\rho_x + v\rho_y + w\rho_z = 0$. Vertical mixing and cross-isobath advection of density are large only in a very narrow region at the shoreward side of the front, precisely where the bottom boundary layer detaches.

These momentum balances show that the flow within the front using MY2 is not quite steady. Furthermore, the lack of mixing suggests that waves could exist there. Indeed, the density and velocities near the bottom within the front oscillate with a period of about 1.3 days (Fig. 5). The amplitudes are small, but the important point is that the flow near the bottom within the front is very different from the case with constant coefficients. In fact, the along-isobath velocity, though small, never vanishes in Fig. 5, whereas the cross-isobath and vertical velocities each reverse during the oscillations.

c. Frontal waves

The oscillatory behavior in Fig. 5 suggests the presence of some type of frontal-trapped waves. Further support is found in a plan view of v just above the bottom (Fig. 6a) and an along-isobath section of v at y

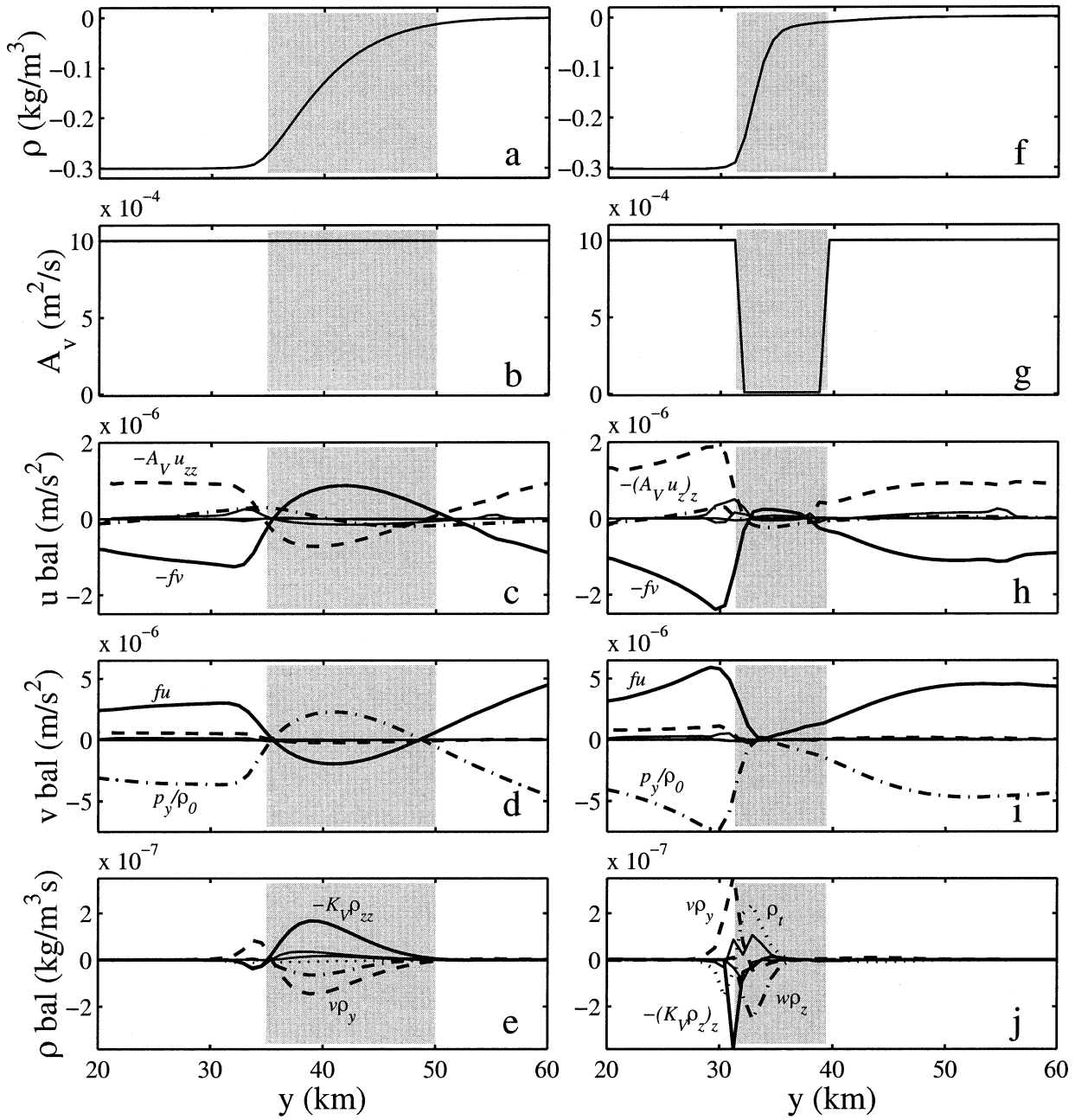

FIG. 4. Density, vertical viscosity, momentum, and density balances along a line parallel to and just above the bottom in Fig. 3 (i.e., within the bottom boundary layer and passing through the front): (left) constant coefficients and (right) MY2. Thick curves are the largest terms: (c) $-fv$ (solid), $-A_V u_{zz}$ (dashed), p_x/ρ_0 (dash–dot); (d) fu (solid), p_y/ρ_0 (dash–dot), $-A_V v_{zz}$ (dashed); (e) $-K_V\rho_{zz}$ (solid), $v\rho_y$ (dashed), $w\rho_z$ (dash–dot); (h) $-fv$ (solid), $-(A_V u_z)_z$ (dashed), p_x/ρ_0 (dash–dot); (i) fu (solid), p_y/ρ_0 (dash–dot), $-(A_V v_z)_z$ (dashed); (j) $w\rho_z$ (dash–dot), ρ_t (dotted), $-(K_V\rho_z)_z$ (solid), $v\rho_y$ (dashed). Thin curves are terms that are essentially negligible. Shading indicates the location of the front.

$= 35$ km (Fig. 6b), which show a bottom-trapped wavelike spatial pattern. The density and momentum balances, along with the wavelike structure, are suggestive of something akin to the baroclinic, bottom-trapped, topographic waves found by Rhines (1970): linear waves in a uniformly stratified fluid (constant buoyancy frequency) within a uniformly rotating, straight channel with vertical walls and a bottom that slopes gently across the channel. The waves are modal in the cross-channel direction but may have any along-channel wavenumber. They decay away from the bottom and always propagate cyclonically (i.e., shallow water on their right in the Northern Hemisphere), obeying a dispersion relation that takes the dimensional form

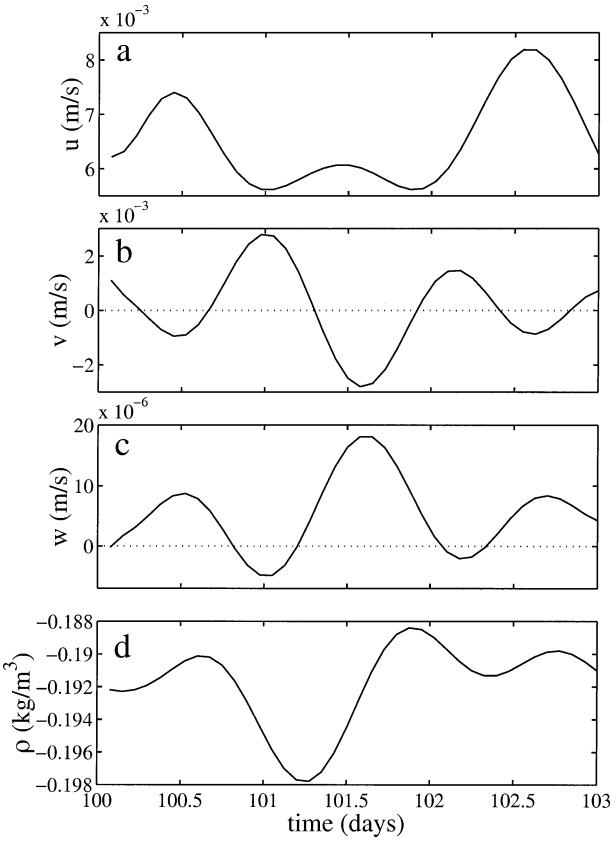

FIG. 5. Time series of (a) along-isobath, (b) cross-isobath, and (c) vertical velocities and (d) density at a point within the front, just above the bottom (x = 145 km, y = 33 km, z = 4 m above the bottom) for the case of MY2 mixing. The front is trapped and has the structure shown in the right panels of Fig. 3.

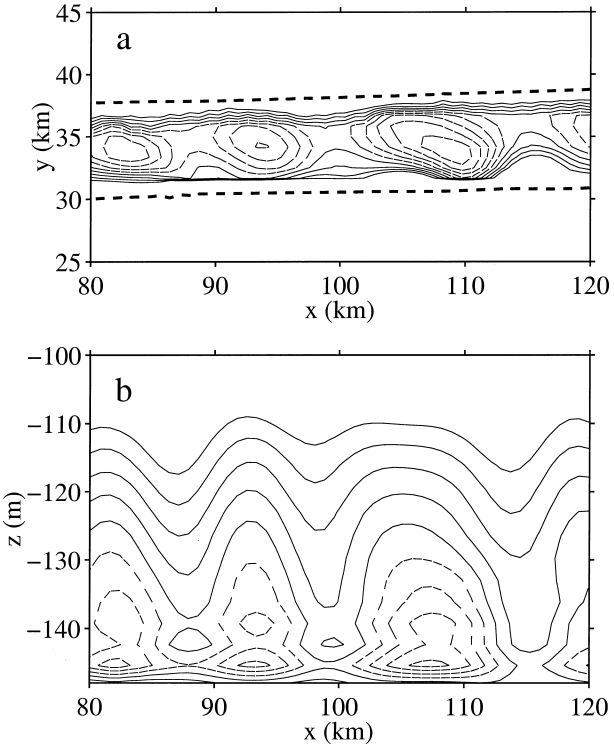

FIG. 6. Cross-isobath velocity v for the case with MY2 mixing. (a) Plan view just above the bottom. (b) Vertical section along the 148-m isobath at y = 35 km. Contour ranges have been restricted to show the structure within the front: (a) −0.004 to 0.002 by 0.0006 m s^{-1}, (b) −0.004 to 0.003 by 0.0007 m s^{-1}. Dashed contours are negative velocities. Thick dashed lines in (a) denote the edges of the front.

$$\sigma = \frac{\alpha k N^2}{f\mu \tanh \mu H}, \tag{3}$$

where

$$\mu^2 = \frac{N^2}{f^2}\left[\left(\frac{n\pi}{L}\right)^2 + k^2\right]. \tag{4}$$

Here, σ is the wave frequency, α is the bottom slope, k is the along-channel wavenumber, N is the buoyancy frequency, μ is the inverse vertical decay scale, H is the mean channel depth, n is the cross-channel mode number, and L is the channel width.

In the present case, the edges of the front appear to act as the channel walls, although they are clearly neither vertical nor solid. Nevertheless, they are treated as vertical walls in order to make a rough comparison with Rhines' (1970) wave solutions. Appropriate estimates of parameters are: $\alpha = 0.005$, $f = 10^{-4}$ s^{-1}, $H = 148$ m is the depth at $y = 35$ km, $L = 8$ km is the width of the front in Fig. 6a, $n = 1$ and $k = (2\pi/13)$ km^{-1} based on Fig. 6a, and $N = 8 \times 10^{-3}$–10×10^{-3} s^{-1} based on the vertical density gradient near the bottom (not shown). Using these values in (3) and (4) produces a vertical decay scale of μ^{-1} = 16–20 m and a wave period of $2\pi/\sigma$ = 1.9–2.4 days. The vertical decay scale is roughly consistent with Fig. 6b; that is, the velocity signal disappears within 2–3 decay scales. On the other hand, the velocity reverses with distance away from the bottom in Fig. 6b, whereas it does not in Rhines' (1970) wave solutions. The theoretical period is 1.5–2 times as long as that shown in Fig. 5, but this difference is not unreasonable considering the differences between the front and the theoretical channel. The frontal waves do propagate cyclonically, although this is not shown here. Despite the differences, the results suggest that the basic dynamics of the frontal waves are probably close to those of the bottom-trapped, topographic waves described by Rhines (1970). A more in-depth analysis is beyond the scope of this note, especially considering that the waves disappear when constant mixing coefficients are used, rendering their existence in nature questionable.

4. Discussion and summary

The sensitivity of the trapped-front model to the parameterization of vertical mixing indicates the need for caution when relating observations to model features. Some features are robust and may be expected to be

observed; others are not robust and should not necessarily be expected. The basic frontal trapping mechanism is apparently robust, suggesting that, to the extent that the model applies to shelfbreak fronts, (1) may provide a good estimate of the frontal attachment depth. The model also implies that such trapped fronts should have a strong surface intensified jet over the front that weakens dramatically toward the bottom. Transport in the bottom boundary layer should approach the front from the shoreward side, with a sharp convergence and detachment at the shoreward edge of the front. This is the most dominant feature of the cross-frontal circulation, which may explain the recent observational support for this feature at the MAB shelfbreak front.

On the other hand, the width and shape of the model front are sensitive to the vertical mixing parameterization and probably cannot be reliably applied to real fronts. Furthermore, the cross-frontal circulation near the bottom within the front is sensitive and, therefore, suspect. With constant coefficients, mixing tends to be strong there, producing steady and smooth cross-frontal circulation with reversed along-isobath flow and onshore flow in the bottom boundary layer. With the MY2 parameterization, mixing tends to be weak within the front, and the flow is unsteady and wavelike. Given the uncertainty of real ocean mixing, it is unclear what cross-frontal velocities to expect. For example, the onshore movement of the dye patch seen by Houghton (1997) is consistent with the onshore flow in the bottom boundary layer of the model with constant coefficients (Fig. 3), but it is also consistent with the temporarily onshore flow of the frontal-trapped waves with MY2 (Figs. 5 and 6). Perhaps either new analyses of existing observations or new measurements will elucidate the flows within the foot of the front, thereby improving our understanding of both shelfbreak front dynamics and mixing. Until then, it is fair to say that it is probably not fruitful to use the trapped-front model alone to quantify properties of shelfbreak fronts that are intimately connected to the cross-frontal circulation, such as cross-frontal exchange.

Numerous additional calculations have been made with other choices for minimum and maximum mixing coefficients, as well as other vertical mixing parameterizations (not shown). All of the results can be understood within the context of those presented here. For example, as the minimum value for the coefficients is increased from 10^{-5} toward 10^{-3} m^2 s^{-1}, mixing becomes more important within the front. The coefficients still change from the maximum outside the front to the minimum within the front, and the balances are intermediate to those in Fig. 4. Larger maximum values have no qualitative effect. They allow a thicker bottom Ekman layer shoreward of the front which tends to produce weaker cross-isobath velocities because the transport is roughly unchanged. A parameterization based on the Richardson number as defined by Yankovsky and Chapman (1997) was also used. This scheme produces a slower transition from maximum to minimum mixing coefficients at the edges of the front, so the flow within the front is a complicated combination of the two extremes presented in Fig. 4. Overall, these additional calculations support the conclusions already stated.

Acknowledgments. I thank Steve Lentz for numerous helpful discussions, comments, and suggestions and Breck Owens, Rich Garvine, and Bob Pickart for their valuable input. Financial support was provided by the Ocean Sciences Division of the National Science Foundation under Grant OCE-9809965 and is gratefully acknowledged.

REFERENCES

Barth, J. A., D. Bogucki, S. D. Pierce, and P. M. Kosro, 1998: Secondary circulation associated with a shelfbreak front. *Geophys. Res. Lett.,* **25,** 2761–2764.

Chapman, D. C., 2000: Boundary layer control of buoyant coastal currents and the establishment of a shelfbreak front. *J. Phys. Oceanogr.,* **30,** 2941–2955.

——, and S. J. Lentz, 1994: Trapping of a coastal density front by the bottom boundary layer. *J. Phys. Oceanogr.,* **24,** 1464–1479.

Garvine, R. W., 1999: Penetration of buoyant coastal discharge onto the continental shelf: A numerical model experiment. *J. Phys. Oceanogr.,* **29,** 1892–1909.

Houghton, R. W., 1997: Lagrangian flow at the foot of a shelfbreak front using a dye tracer injected into the bottom boundary layer. *Geophys. Res. Lett.,* **24,** 2035–2038.

——, and M. Visbeck, 1998: Upwelling and convergence in the Middle Atlantic Bight shelfbreak front. *Geophys. Res. Lett.,* **25,** 2765–2768.

Loder, J. W., B. Petrie, and G. Gawarkiewicz, 1998: The coastal ocean off northern North America: A large-scale view. *The Sea,* K. H. Brink and A. R. Robinson, Eds., The Global Coastal Ocean: Regional Studies and Syntheses, Vol. 11, John Wiley and Sons, 105–133.

Mellor, G. L., and T. Yamada, 1982: Development of a turbulence closure model for geophysical fluid problems. *Rev. Geophys. Space Phys.,* **20,** 851–875.

Pickart, R. S., 2000: Bottom boundary layer structure and detachment in the shelfbreak jet of the Middle Atlantic Bight. *J. Phys. Oceanogr.,* **30,** 2668–2686.

Rhines, P. B., 1970: Edge-, bottom-, and Rossby waves in a rotating stratified fluid. *Geophys. Fluid Dyn.,* **1,** 273–302.

Sanford, T. B., and R.-C. Lien, 1999: Turbulent properties in a homogeneous tidal bottom boundary layer. *J. Geophys. Res.,* **104,** 1245–1257.

Stahr, F. R., and T. B. Sanford, 1999: Transport and bottom boundary layer observations of the North Atlantic Deep Western Boundary Current at the Blake Outer Ridge. *Deep-Sea Res.,* **46B,** 205–243.

Yankovsky, A. E., and D. C. Chapman, 1997: A simple theory for the fate of buoyant coastal discharges. *J. Phys. Oceanogr.,* **27,** 1386–1401.